Buckling and flow alignment in foliated rock

H. B. Muhlhaus, Frédéric Dufour, L. Moresi, B. Hobbs, H. Sakaguchi

Buckling and flow alignment in foliated rock

H-B Mühlhaus, F. Dufour, L.Moresi, B.E. Hobbs, H. Sakaguchi

CSIRO Division of Exploration and Mining, Australian Resources Research Centre, PO Box 1130, Bentley, 6102 Western Australia (email: hans@ned.dem.csiro.au)

Abstract

A model for finely layered visco-elastic rock proposed by us in previous papers is used as the basic unit for a granular rock. The grains are distinguished by individual layer orientations. Initially the layer orientations are randomly distributed. Size effects are considered within the framework of a couple stress theory. We begin with an outline of the governing equations for the standard continuum case and apply a computational simulation scheme suitable for problems involving very large deformations. We then revisit buckling instabilities in a finite, rectangular domain considered in previous papers. Embedded within this domain, parallel to the longer dimension we consider a stiff, layered beam under compression. We analyse folding up to 40% shortening. In the case of viscoelasticity we observe significant mode coupling in the nonlinear range, a second dominant wavelength emerges around 30-40%axial shortening in a rather spectacular way. We propose to consider size effects due to internal structure (the thickness of the individual layers) within the framework of a couple stress theory. Couple stress theories involve second order spatial derivatives of the velocities/displacements in the virtual work principle. To avoid C_1continuity in the finite element formulation we introduce the spin of the cross sections of the individual layers as an independent variable and enforce equality to the spin of the unit normal vector to the layers (-the director of the layer system-) by means of a penalty method. We illustrate the convergence of the penalty method by means of numerical solutions of simple shears of an infinite layer for increasing values of the penalty parameter. For the shear problem we present solutions assuming that the internal layering is oriented orthogonal to the surfaces of the shear layer initially. For high values of the ratio of the normal–to the shear viscosity the deformation concentrates in thin bands around to the layer surfaces. Also in the context of simple shear we associate different initial director (=normal vector to the internal layer planes) orientations to each particle of our particle advection finite element scheme. The initial distribution of director orientations is random. We then demonstrate the emergence of a schistose rock-like material in the course of finite simple shearing.

Introduction

We explore scenarios from global to internal buckling in nonlinear finite element studies. Numerical solutions based on the standard continuum formulation assumed initially become unstable if the contrast between the normal and the shear viscosity becomes very severe. As a remedy for the latter situation and also as a means to consider internal structure we derive a couple stress formulation, which is numerically robust in such cases as well. We illustrate the couple stress model by means of numerical solutions of simple, finite shear of an infinite layer, revisit the folding problem in the light of the couple stress theory and illustrate flow alignment in the context of simple shear for initially randomly oriented layer orientations.

Mathematical formation

Initially we assume linear viscous behaviour and designate with h the normal viscosity and h_S the shear viscosity in the layer planes normal to n_i. The orientation of the normal vector, or director as it is sometimes called in the literature on oriented materials, changes with deformation. Using a standard result of continuum mechanics, the evolution of the director of the layers is described by

$$\overset{\circ}{n}_i = W^n_{ij} n_j \text{ where } W^n_{ij} = W_{ij} - (D_{ki}\lambda_{kj} - D_{kj}\lambda_{ki}) \text{ and } \lambda_{ij} = n_i n_j \tag{1}$$

where **L**=**D**+**W** is the velocity gradient, **D** is the stretching and **W** is the spin. The superscriped n distinguishes the spin $\boldsymbol{W}^n$ of the director $\boldsymbol{n}$ (the unit normal vector of the deformed layer surfaces) from the spin $\boldsymbol{W}$ of an infinitesimal volume element dV of the continuum. The 2D matrix representation of (1) as needed for our computational applications is represented in appendix A2 for easy reference. We define a corotational stress rate as:

$$\overset{\circ}{\sigma}{}^n_{ij} = \overset{\circ}{\sigma}_{ij} - W^n_{ik}\sigma_{kj} + \sigma_{ik}W^n_{kj} \tag{2}$$

Again the superscripted n distinguishes the stress rate $\overset{\circ}{\sigma}{}^n$ as observed by a material observer co-rotating with the director $\boldsymbol{n}$ from the material stress rate $\overset{\circ}{\sigma}$ observed by a spatially fixed observer.

Specific viscous and viscoelastic constitutive relations

We consider layered, viscous and visco-elastic materials. The layering may be in the form of an alternating sequence of hard and soft materials or in the form of a superposition of layers of equal width of one and the same material, which are weakly bonded along the interfaces. We designate the normal shear modulus and the normal shear viscosity as μ and η respectively; the shear modulus and the shear viscosity measured in simple, layer parallel shear we designate as μ_S and η_S.

In the following simple model for a layered viscous material we correct the isotropic part $2\eta D'_{ij}$ of the model by means of the Λ tensor (see appendix A1 for derivation) to consider the mechanical effect of the layering; thus

$$\sigma_{ij} = 2\eta D'_{ij} - 2(\eta - \eta_S)\Lambda_{ijlm}D'_{lm} - p\delta_{ij} \tag{3}$$

where a prime designates the deviator of the respective quantity, and

$$\Lambda_{ijkl} = (\frac{1}{2}(n_i n_k \delta_{lj} + n_j n_k \delta_{il} + n_i n_l \delta_{kj} + n_j n_l \delta_{ik}) - 2 n_i n_j n_k n_l). \quad (4)$$

Similarly, a visco-elastic constitutive relationship for a layered medium may be written as:

$$D'_{ij} = \frac{1}{2\mu} \overset{\nabla n}{\sigma}{}'_{ij} + \frac{1}{2\eta} \sigma'_{ij} + (\frac{1}{2\mu_S} - \frac{1}{2\mu}) \Lambda_{ijkl} \overset{\nabla n}{\sigma}{}'_{kl} + (\frac{1}{2\eta_S} - \frac{1}{2\eta}) \Lambda_{ijkl} \sigma'_{kl} \quad (5)$$

where $\overset{\nabla n}{\sigma}_{ij}$ is the co-rotational stress rate introduced at the beginning of this section. We could have equally well used the Jaumann derivative of σ which is obtained by replacing $\mathbf{W}^n$ in (2) by the spin of an infinitesimal element of the continuum **W**. A remark on the notation: We use index notation which is less ambiguous than symbolic notation when vectors, second and fourth order tensors (such as Λ_{ijkl}) appear simultaneously in the equations.

The particle-in-cell finite element method

Some difficulties arise in devising a practical implementation of the finite element formulation described in section 3 for the large deformation modeling of layer folding. In particular, since the **C** matrix is a continuously evolving function of position through its dependence on director orientation, it is necessary that we are able to track an evolving vector function of the material during deformation.

We have therefore developed a hybrid approach –a particle-in-cell finite element method that uses a standard Eulerian finite element mesh (for fast, implicit solution) and a Lagrangian particle framework for carrying details of interfaces, the stress history etc.

Our particle-in-cell finite element method is based closely on the standard finite element method, and is a direct development of the Material Point Method of Sulsky *et al.* (1995). The standard mesh is used to discretize the domain into elements, and the shape functions interpolate node points in the mesh in the usual fashion. The problem is formulated in a weak form to give an integral equation, and the shape function expansion produces a discrete (matrix) equation. For the discretized problem, these integrals occur over sub-domains (elements) and are calculated by summation over a finite number of sample points within each element. For example, in order to integrate equation the stiffness matrix of our finite element scheme, over the element domain Ω^E e we replace the continuous integral by a summation

$$\mathrm{Z}\,\mathbf{K}^E = \sum_p w_p \mathbf{B}^T(\mathbf{x}_p) \mathbf{C}_p(\mathbf{x}_p) \mathbf{B}(\mathbf{x}_p) \quad (6)$$

In standard finite elements, the positions of the sample points, $\boldsymbol{x}_p$, and the weighting, w_p are optimized in advance. In our scheme, the $\boldsymbol{x}_p$'s correspond precisely to the Lagrangian points embedded in the fluid, and w_p must be recalculated at the end of a time step for the new configuration of particles. Constraints on the values of w_p come from the need to integrate polynomials of a minimum degree related to the degree of the shape function interpolation, and the order of the underlying differential equation (e.g Hughes,1987). These Lagrangian points carry the history variables including the director orientation which are therefore directly

available for the element integrals without the need to interpolate from nodal points. Moresi et al. (2001) give a full discussion of the implementation of the particle-in-cell finite element scheme used here including full details of the integration scheme and its assumptions.

Numerical simulations

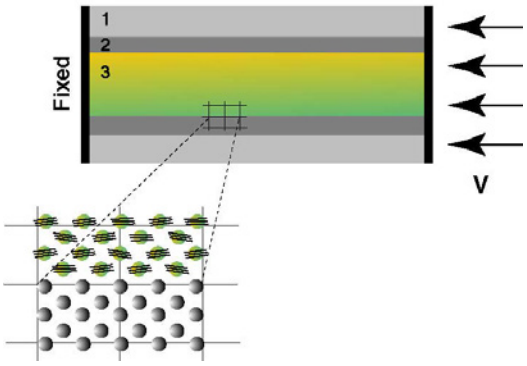

*Figure 1. Initial geometry for the folding experiment. Layer 1 is compressible, viscous (η_M) background material, layer 2 is identical to layer 1 but incompressible (see text for an explanation), layer 3 is the test sample: viscoelastic (μ, μ_S, η, η_S) with a director orientation (**n**). The anisotropic layer contains small perturbations to the otherwise horizontal internal layering. V=10 is constant during any given experiment and unchanged between different experiments. The length of the block is L=2 and the width of the central layer 3 is h=0.12.*

We present an example of a simulation of folding of a layer of anisotropic viscous material sandwiched between two isotropic layers of equal viscosity (Figure 1). To accommodate the shortening of the system, one of the isotropic layers is compressible. In benchmarking this sandwich of incompressible and compressible embedding material was found to give good agreement with analytic results assuming an infinite domain (Moresi et al, 2001). The Debora number *De* (relaxation time/process time) is defined as $De = (\eta V)/(\mu L)$. We consider the cases in *De= 0.5* and *5* respectively. We assume that $\eta / \eta_S = \mu / \mu_S$. The folding process is triggered by initial perturbations of the form $\delta x_2 = 0.05h\cos(qx_1)$, $0 \le x_1 \le 2$.

In both cases, $De = (\eta V)/(\mu L)$ =5 and 0.5 respectively we observe for the large wavelength perturbation no or at least no significant mode coupling: the initial perturbation is amplified in an unstable fashion. The growth coefficient of the homogeneous rectilinear ground solution is $L/V = 0.2$ would produce an amplification of the initial perturbation of about 4.5 at 40%shortening which is much smaller than what we observe for the long wavelength perturbations in case of the viscous layers and for both short and long wavelength perturbations in the viscoelastic cases. A second, dominant mode emerges at q=10p in case 4 in a rather spectacular way between 25-35% shortening (Figure 2).

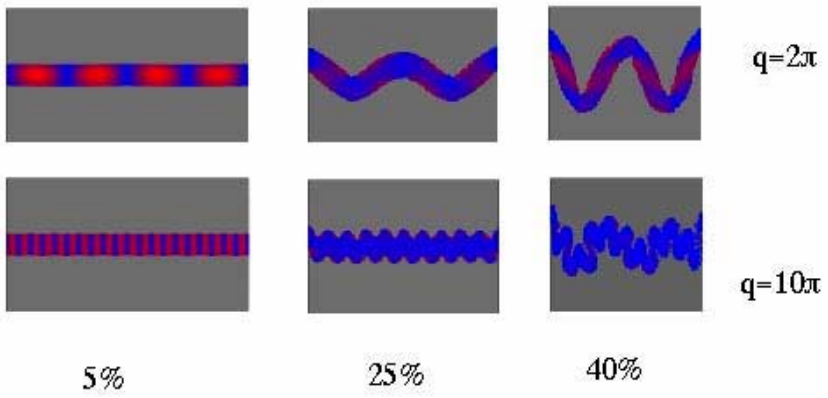

Figure 2. Evolution of folding in anisotropic viscoelastic layer. $De = (\eta V)/(\mu L) = 5$ *. Isotropic embedding material has viscosity 1, layer has shear viscosity 10, normal viscosity 1000 and* $\eta / \eta_S = \mu / \mu_S$ *. Results are shown for perturbation to the director orientation with wavenumber* $q = 2\pi$ *and* $q = 10\pi$

A more viscous case with *De=0.5* is represented in Figure 3.

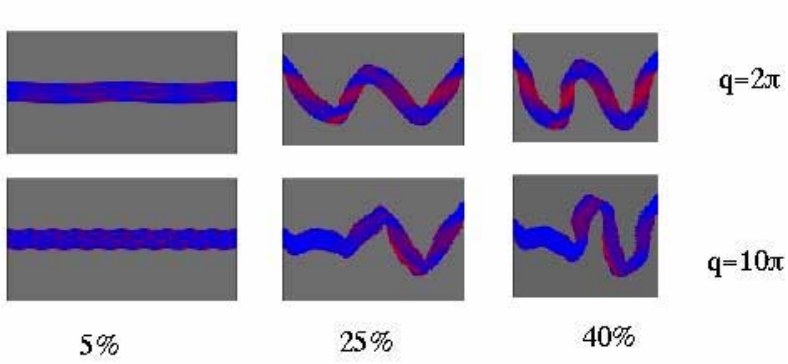

Figure 3. Case 4 Evolution of folding in anisotropic viscoelastic layer. $De = (\eta V)/(\mu L) = 0.5$ *. Isotropic embedding material has viscosity 1, layer has shear viscosity 10, normal viscosity 1000 and* $\eta / \eta_S = \mu / \mu_S$ *. Results are shown for perturbation to the director orientation with wavenumber* $q = 2\pi$ *and* $q = 10\pi$

Couple Stresses

Couple stresses are significant in situations where the gradient of n_i changes strongly over a short distance (limiting case: disinclination).

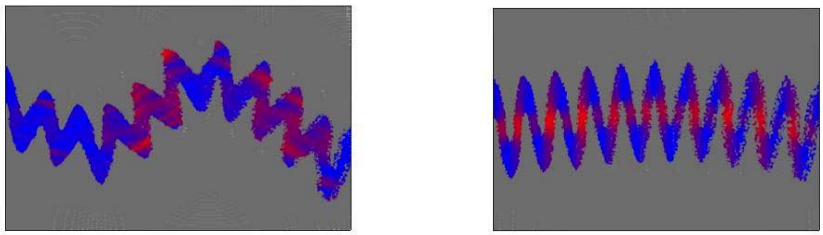

(a) (b)

Figure 4. Evolution of folding in viscous layer. Isotropic embedding material has viscosity 1, layer has, normal viscosity 1000. Results are shown for perturbation to the director orientation with wavenumber $q = 10\pi$ at 40% shortening. (a) layered beam, $\eta / \eta_S = 1000$ (b) couple stresses included , same as (a) otherwise.(Layer thickness)/(beam thickness)=0.2. In this example the internal length was chosen relatively large hence the Cosserat terms act on the larger wavelengtht, increase the larger length scale. The effect of couple stresses in connection with higher values of the shear viscosity and in particular in the the context of viscoelasticity requires further investigation

In such cases we have to take the variations of the normal stresses across the layer cross sections into consideration (e.g. Mühlhaus, 1993). The couple stress theories (see e.g. Mindlin and Thiersten, 1962; Mühlhaus, 1993; Mühlhaus & Aifantis, 1991a,b) provide a convenient framework for the consideration of stress fluctuations on the layer-scale without having to abandon the homogeneity properties of the anisotropic standard continuum approach. In the present case the couple stress enhancement leads naturally to the superposition of visco-elastic bending stiffness on our standard continuum model. In connection with layered materials the internal length scale introduced by the couple stresses is proportional to the layer thickness (ranging from microns to kilometers in geological applications) and to the differences between the viscosities and shear moduli governing pure and simple shear respectively (see e.g. Mühlhaus, 1993). In layered materials the explanation why the stress tensor is non-symmetric in couple stress materials is straight forward: In a continuum description the stresses represent average values over multiples of the layer thickness. In bending the shear stress obtained by averaging normal to the layering is different in general from the shear stress parallel to the

layering. The latter is even zero for instance in the case of a stack of perfectly smooth cards (a standard continuum model would break down in this case). Within the framework of a couple stress theory one considers the variation of the normal stress across the layer thickness (in much the same way as in the standard engineering beam and plate theories), introduces statically equivalent couple stresses balancing the difference between the shear stresses.

The couple stress tensor $\boldsymbol{\mu}$ (moment per unit area) is conjugate in the rate of energy to the rate of curvature $\hat{\boldsymbol{\kappa}}$. In the context of layered materials, a natural choice for the rate of curvature reads:

$$\hat{\boldsymbol{\kappa}} = \boldsymbol{\varphi}\nabla \quad \text{where } \boldsymbol{\varphi} = \mathbf{n}\times\dot{\mathbf{n}}. \tag{7}$$

In 2D deformations in the (x_1, x_2) plane if the director is parallel to the x_2 axis, (14) reduces to

$$\kappa_{31} = v_{2,11} \text{ and } \quad \kappa_{32} = v_{2,12} \tag{8}$$

The power balance for a couple stress medium reads:

$$\int_V (\sigma_{ij} D_{ij} + \mu_{ij}\kappa_{ij})dV = \int_V \rho((b_i - \dot{v}_i)v_i + (m_i^V - \dot{d}_i)\varphi_i)dV + \int_S (t_i v_i + m_i^S \varphi_i)dS \tag{9}$$

where the superscripted dot means differentiation with respect to time, $\dot{d}_i$ is the angular momentum, b_i and m_i^V are volume forces and couples respectively ,

$$t_i = (\sigma_{ij} - \mu_{ij,kk})N_j \text{ and } m_i^S = \mu_{ij}N_j \tag{10}$$

are the surface stress and couple stress tractions and N_i is the unit outward normal vector to the surface S of the body. There are a number of complications associated with the application of couple stress theories in finite element analyses. For instance rotations cannot independently varied on surfaces where the normal component of the displacements or velocities are prescribed. In this case the velocity gradients on the surface have to be decomposed into normal and surface parallel components. The surface parallel part will- after application of the surface divergence theorem- produce a contribution to the stress traction (see e.g. Muhlhaus and Aifantis (1991) and Fleck and Hutchinson (1997) for details of the analysis within the context of a strain gradient- and a couple stress theory respectively). Another difficulty arises from the fact that that the volume integrals in (9) contain second order velocity gradients so that the shape functions in a finite element model must be continuously differentiable across element boundaries (C_1 continuity). Standard finite element programs mostly support C_0 continuity only. Both problems, the non-independence of variations of surface gradients and the C_1 continuity, can be circumvented by relaxing the constraint

$$W_{ij}^n + e_{ijk}\varphi_k = 0 \tag{11}$$

in the spirit of a penalty approach (see (1) for definition of W_{ij}^n) by adding the term

$$\int P(W_{ij}^n - W_{ij}^c)(W_{ij}^n - W_{ij}^c)dV \quad \text{, where } W_{ij}^c = -e_{ijk}\varphi_k \tag{12}$$

to the lhs of (9). In (12) P is the so called penalty parameter. If the energy supply is bounded then we expect that the original constraint (11) will be satisfied in the limit as $P \to \infty$. In the relaxed form of the governing equations we have recovered the equations of the full (unconstrained) Cosserat continuum where the rotations φ_i are independent degrees of freedom. In our case this is true as long as P is finite. The independence of the rotations means that the non-independence of surface gradients and the C_1 continuity problem have disappeared. In finite element calculations the velocities and rotations are approximated independently and since the highest order derivative of both velocities and rotations are of the first order (in the power balance) both may be approximated by using the same type of shape function, which needs to be C_0 continuous only.

For illustration of the model we consider the simple shearing of an infinite, viscous layer $(x_1, 0 \le x_2 \le h)$. On the surface $x_2 = h$ the shear stress $\sigma_{12} = \tau = const$ is prescribed and we assume that $\sigma_{22} = 0$. Also at $x_2 = h$ we assume that $\varphi_3 = 0$ and we designate the local, unknown velocity as V. At $x_2 = 0$ we assume that $v_1 = v_2 = \varphi_3 = 0$. The initial director orientation is $\mathbf{n}^T = (1,0)$ i.e. initially the material layer surfaces are oriented orthogonal to the surfaces of the shear layer. First we consider the convergence of the penalty scheme for increasing values of the penalty parameter P. Figure 5 shows the dimensionless velocity $\bar{V} = V\eta_S/(\tau h)$ as a function of the dimensionless parameter $\bar{P} = P/\eta_S$ for three cases: analytic solution, finite element solution assuming full numerical integration and a finite element solution using one point integration for the integration of the penalty stiffness terms. The analytic- and the one-point numerical solution coincide to the first three digits , however the finite element solution based on full integration diverges for increasing values of the penalty parameter: the velocity on top tends to zero. The reason for the divergence is that for the present choice of finite elements (4 noded quadrilaterals, periodic boundary conditions on the sides) $\mathbf{W}^n$ is constant within an element whereas $\mathbf{W}^c$ is linearily variable. The latter produces to a positive definite contribution to the argument of the penalty stiffness depending quadratically on x_2.

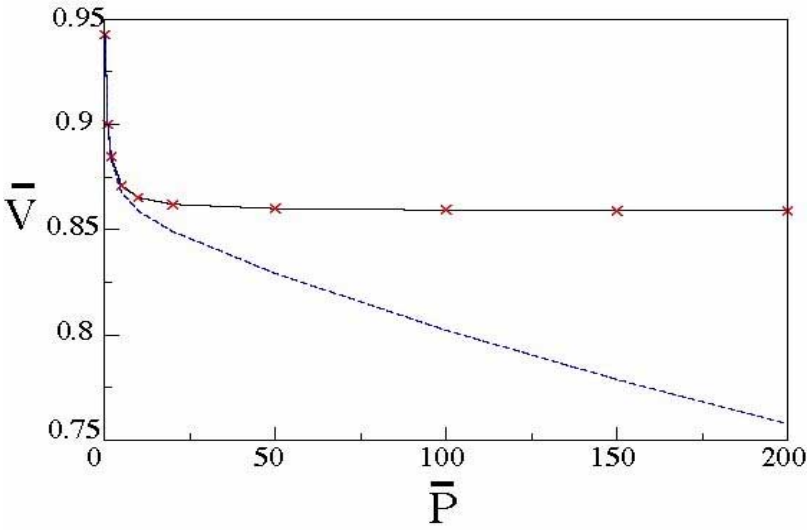

Figure5. Dimensionless velocity $\bar{V} = V\eta_S/(\pi h)$ *versus dimensionless penalty parameter* $\bar{P} = P/\eta_S$ *; analytical solution (crossed); numerical, full integration (broken line); numerical, one point integration (solid line). Finite element model: eight by twelve four noded quadrilaterals; sixteen particles per element. Periodic boundaries on the sides, i.e. velocities and rotations are the same on both sides; if one particle leaves the domain on one side it re-appears on the other side.* $\eta/\eta_S = 2$ *, t/h=0.2; t=thickness of the individual layers and h is the thickness of the shear layer. During the calculation the director orientation is fixed at* ***n*** *=(1,0) , i.e. the internal layering is always orthogonal to the* x_2*=const.*

In Figure 5 we show the evolution of $\bar{V}$ as a function of the director orientation as described by the angle $\Phi_0 = \Phi_3(x_2 = 0)$ between the x_2 axis and **n** and the evolution of the dimensionless Cosserat rotation (see Figure caption for definition) at the center of the shear layer respectively.

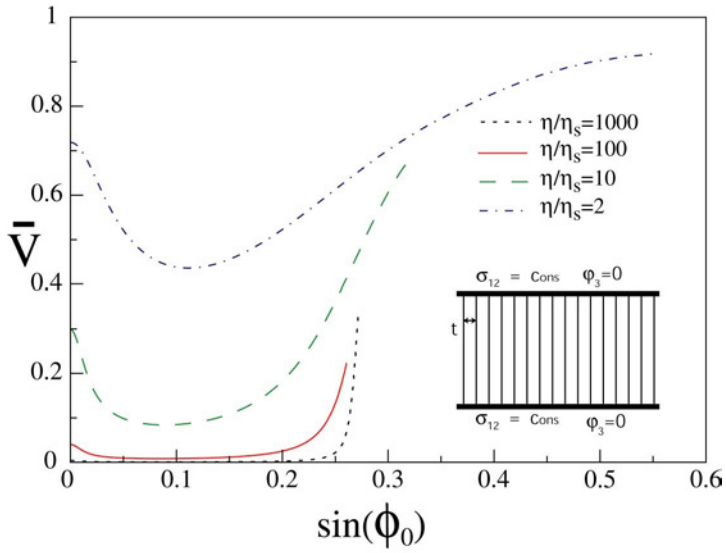

Figure 5. $\bar{V}$ *as a function of* $\sin(\Phi_0)$, $\Phi_0 = \Phi_3(x_2 = 0)$. *t/h= 0.2*

An interesting application of our layered model arises is initially we assign random director orientations to each particle of our particle advection scheme. In this case the model material is macroscopically isotropic initially. Internal reorientations, the evolution of textures are described by the director evolution equation (1). Results for the simple shear problem considered before are shown in Figure 6.

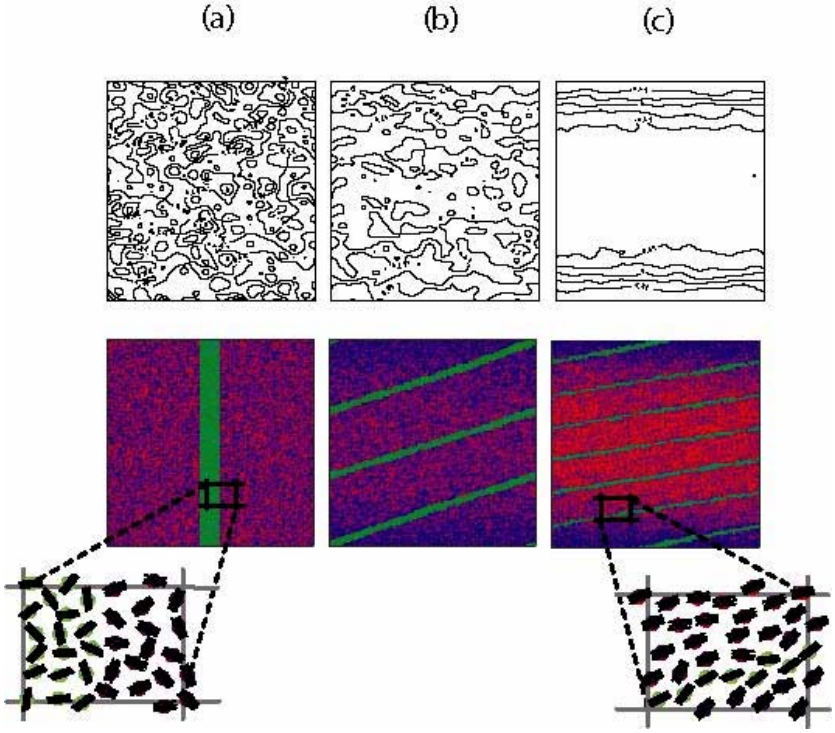

Figure 6 Simple shear, same boundary conditions as in previous example however the director orientations are initially random: every particle of our advection scheme gets its own spatially randomly distributed director orientation; Φ *= angle between the* x_2 *and the director orientation ranges between p/2 and - p/2. The top row are contour lines of* Φ *. The deformation increases from (a) to (b). The green line (bottom) row, Figures (a)-(c) show initial and displaced particle positions. The parallel lines in (b) and (c) follow from the periodic boundary conditions*

Conclusions

We have presented a simple formulation for the simulation of large, viscoelastic deformations in layered systems. The influence of the bending stiffness of the individual layers is considered within the framework of a couple stress theory. The combination of the basic model with a large deformation, particle-in-cell finite element method allows the simulation of a diverse range of crustal deformation problems. By way of examples we have given a realistic treatment of folding and simple shear processes, which includes the mechanical influence of fine-scale. The model is relatively simple in its present form but still gives a useful insight into the physical processes involved in certain types of folding processes involving simple shear.

One of the most interesting results occurs for purely viscous, layered simulations where low-wavenumber folding is induced even for very low viscosity contrasts between embedded and embedding media. In the past, the very large viscosity contrasts required to produce Biot-type folding in purely viscous media have led people to discount the possibility that viscous buckling occurs at all in geology.

In folding couple stresses have an appreciable effect only if the ratios of the parameters (layer material/embedding material; normal viscosity/shear viscosity etc) are very extreme, e.g. equal to 1000 or more. In the case of the shear layer the influence of couple stresses appreciable already at relatively low parameter ratios as long as the ratio of the thickness of an individual layer to the width of the shear layer is of the order of 1/10 or more. If couple stresses are considered the deformation of the layer is no longer homogeneous; we observe, depending on the viscosity ratio the formation of a slowly deforming core, rapid shearing concentrates around the layer surfaces. An interesting application of the layered model arises if director orientations are assigned at random to the particles of the advection scheme initially. The material is then macroscopically isotropic initially; texture such as schistosity evolve in the course of the deformation.

References

Fleck, N.A. and Hutchinson, J.W. 1997 Strain gradient plasticity. Advances in Applied Mechanics, Vol. 13. 295-361

Fletcher, R.C. 1974. Wavelength Selection in the Folding of a Single Layer with Power Law Rheology. Am. J. Sci. Vol 274. 1029-1043

Fletcher, R.C. 1982. Coupling of diffusional mass transport and deformation in tight rock. Tectonophysics, Vol. 83. 275-291

Hill, R. and Hutchinson, J.W. 1975. Bifurcation Phenomena in Plane Tension Test. J. Mech. Phys. Solids. Vol. 23. 239-264

Hobbs, B.E., Muhlhaus,H-B, Ord, A and Moresi, L. (2001) The Influence of Chemical migration upon Fold Evolution in Multi-layered Materials. Vol. 11, Yearbook of Self Organisation. Eds H.J. Krug and J.H. Kruhl.

Hobbs, B.E., Means, W.D. and Williams, P.F. 1976.An Outline of Structural Geology. Wiley

Hunt, G.W., Muhlhaus, H-B and Whiting, A.I.M. (1997). Folding processes and solitary waves in structural geology. Phil. Trans.of R. Soc. London, 355, 2197-2213.

Johnson, A.M. and Fletcher, R.C. (1994) Folding of Viscous Layers. Columbia University Press, New York

Mindlin, R.D. and Thiersten, H.F. 1962. Effects of couple stresses in linear elasticity. Arch. Rat. Mech. Analysis. Vol. 11. 415-448

Moresi, L., Muhlhaus, H.-B., Dufour, F. 2001. Particle- in-Cell Solutions for Creeping Viscous Flows with Internal Interfaces . In: Proceedings of the 5th International Workshop on Bifurcation and Localization in Geomechanics (IWBL'99), Perth, W. A., Australia. Ed's: H-B Muhlhaus, A Dyskin and E Pasternak Australia, Balkema, Rotterdam.To appear: Dec2000

Mühlhaus, H.-B., Aifantis, E.C. 1991a. A variational principle for gradient plasticity. Int. J. Solids and Structures. Vol. 28. 845-857

Mühlhaus, H.-B., Aifantis, E.C. 1991b. The influence of microstructure-induced gradients on the localization of deformation in viscoplastic materials. Acta Mechanica Vol. 89. 217-231.

Mühlhaus, H.-B. 1993. Continuum models for layered and blocky rock. In: Comprehensive Rock Engineering. Invited Chapter for Vol. II:Analysis and Design Methods. Pergamon Press. 209-230.

Muhlhaus, H-B, Moresi, L, Hobbs, B. E., Dufour, 2001, Large amplitude folding in finely layered viscoelastic rock structures, Pure Applied Geophys, In press. http://www.ned.dem.csiro.au/research/solidmech/Publications

Schmalholz, S.M. and Podladchikov, Y. 1999. Buckling versus folding: Importance of Viscoelasticity. Geophysical Research Letters, Vol. 26, 17, 2641-2644

Sulsky, D., Zhou, S.-J., Schreyer, H. L. 1995. Application of a Particle-in-Cell Method to Solid Mechanics, Comput.Phys. Commun. 87, 236-252.

Vasilyev, O.V., Podladchikov, Y.Y. and Yuen, D. A. 1998. Modelling of compaction driven flow in poro-viscoelastic medium using adaptive wavelet collocation method, Geophysical Research Letter, 17, 32-39